



## Identification of photoelectron energy peaks in Saturn's inner neutral torus

P. Schippers,<sup>1,2,3</sup> N. André,<sup>1,2,4</sup> R. E. Johnson,<sup>5</sup> M. Blanc,<sup>1,2</sup> I. Dandouras,<sup>1,2</sup> A. J. Coates,<sup>6</sup> S. M. Krimigis,<sup>7</sup> and D. T. Young<sup>8</sup>

Received 17 April 2009; revised 6 August 2009; accepted 9 September 2009; published 18 December 2009.

[1] We present observations from the Cassini Plasma Electron Spectrometer (CAPS/ELS) of characteristic peaks in the electron energy spectrum that are identified in the innermost regions of the Saturnian magnetosphere during low-latitude orbits of the Cassini spacecraft around Saturn. We show how a narrow electron energy peak at about 20 eV and a possible peak at about 42 eV can be extracted from the background in CAPS observations after the contamination from high-energy particles has been removed from the measurements. We estimate the density of the newly discovered electron population to be a small fraction (10%) of the electron density measured in the CAPS/ELS energy range, and a much smaller fraction (about 1%) of the total electron density measured by Radio and Plasma Wave Science since our measurements are affected by spacecraft negative potential. We suggest that this population corresponds to photoelectrons generated by the solar EUV photoionization of the extended cloud of neutral gas observed in these regions. We use pitch angle information to assess the near-equatorial source of these photoelectrons and a simple model of chemistry in order to further support our interpretation. Therefore, photoionization seems to be an additional process for plasma production in the innermost Saturnian magnetosphere. Finally, we mention that the comparison of the modeled and the observed photoelectron peak energies could be used to estimate the spacecraft potential in this region which is measured independently by the Langmuir Probe.

**Citation:** Schippers, P., N. André, R. E. Johnson, M. Blanc, I. Dandouras, A. J. Coates, S. M. Krimigis, and D. T. Young (2009), Identification of photoelectron energy peaks in Saturn's inner neutral torus, *J. Geophys. Res.*, *114*, A12212, doi:10.1029/2009JA014368.

### 1. Introduction

[2] The Saturnian inner magnetosphere between 2 and 8 Saturn radii ( $1 R_s = 60,268$  km) is immersed in a very extended cloud of neutral gas [Shemansky and Hall, 1992; Shemansky et al., 1993; Esposito et al., 2005], dominated by hydrogen and products of water dissociation, and whose density exceeds the local plasma density almost everywhere by at least one order of magnitude [Jurac and Richardson,

2007]. These dominant populations of atoms and molecules give the Saturnian magnetosphere its unique character amongst other planetary magnetospheres in the Solar System.

[3] Before the arrival of the Cassini spacecraft at Saturn, the main sources of the observed extended cloud of neutral gas was believed to be Saturn's icy moons and ice grains, with sputtering suggested to be the main mechanism for populating this cloud [Jurac et al., 2001]. The new Cassini measurements actually identified unambiguously the principal source and revealed that active venting at the south pole of Enceladus was responsible for the release of a plume of neutral gas and dust that fill the Saturnian environment [Dougherty et al., 2006; Hansen et al., 2006; Porco et al., 2006; Tokar et al., 2006]. The observed plume is predicted to produce a radially narrow and dense torus of water-group neutral atoms and molecules centered on Enceladus' orbit, the Enceladus torus, with charge-exchange processes within the Enceladus torus producing the very extended cloud of neutral gas observed in the inner Saturnian magnetosphere up to  $\sim 8 R_s$  [Johnson et al., 2006a]. At its inner boundary, at about  $\sim 2 R_s$ , a large fraction of these neutrals, as well as plasma species [Farrell et al., 2008], may be absorbed by the Saturnian main ring particles [Jurac and Richardson, 2007], but a ring ionosphere/atmosphere has been detected

<sup>1</sup>Université de Toulouse, UPS, CESR, Toulouse, France.

<sup>2</sup>UMR 5187, CNRS, Toulouse, France.

<sup>3</sup>Now at Department of Physics and Astronomy, University of Iowa, Iowa City, Iowa, USA.

<sup>4</sup>Research and Scientific Support Department, SRE-SM, ESTEC, European Space Agency, Noordwijk, Netherlands.

<sup>5</sup>Engineering Physics, University of Virginia, Charlottesville, Virginia, USA.

<sup>6</sup>Mullard Space Science Laboratory, University College London, Surrey, UK.

<sup>7</sup>Johns Hopkins University Applied Physics Laboratory, Laurel, Maryland, USA.

<sup>8</sup>Southwest Research Institute, San Antonio, Texas, USA.

during Saturn Orbit Insertion [Tokar et al., 2005; Coates et al., 2005; Johnson et al., 2006b].

[4] Electrons play an important role in many aspects of the physicochemical processes that take place in the Saturnian inner magnetosphere, which is dominated by neutral/plasma interactions and possibly by dust/plasma interactions [Wahlund et al., 2009]. The sources and losses of different plasma constituents are ionization of neutrals, charge exchange, recombination and dissociation [Blanc et al., 2002]. Electrons are produced by photoionization of neutrals and dust, by electron impact on neutrals and by energetic particle impact on water rich dust grains. In the photoionization process of neutrals, electrons are produced at well-defined energies (excess energies), which corresponds to the energy of the EUV solar photon minus the binding energy of the neutral atomic or molecular species [Huebner et al., 1992]. In the electron-impact ionization process on neutrals, one hot electron hits a neutral, resulting in its ionization and the emission of two electrons: a low energy electron (cold electron at a few eV) and an intermediate energy electron (warm electron with energy lower than the incident) [Santos-Costa et al., 2007]. The efficiency of this process depends on the electron-impact cross section of the neutral species, and on the energy of the incident hot electron. This process thus generally produces a broader electron energy spectrum than the photoionization process. The spectral electron characteristics (energy, width, intensity) and fluid parameters (density, temperature) can serve as tracers of the parent neutral species present in the environment.

[5] Photoelectrons generated from the ionization of planetary atmospheres by solar EUV photons are expected to be detected in any planetary atmosphere. Ionospheric photoelectrons have been observed directly at Earth [Coates et al., 1985, and references therein], and more recently at Mars [Frahm et al., 2006] and Venus [Coates et al., 2008], as well as in the Saturnian ring exosphere [Coates et al., 2005] and at Titan [Coates et al., 2007].

[6] In this study, we present detailed observations from CAPS/ELS of characteristic peaks in the electron energy spectrum that are identified in the innermost regions of the Saturnian magnetosphere. We characterize the properties of the corresponding electron populations and interpret them as photoelectrons generated by solar EUV photoionization of the extended cloud of neutral gas observed in these regions. Our newly reported observations should be included in future attempts to model the neutral and plasma environment of Saturn, in addition to the charge exchange [Tokar et al., 2008] and the electron-impact [Delamere and Bagenal, 2008] mechanisms.

## 2. Instruments and Method

### 2.1. CAPS/ELS and MIMI/LEMMS Instruments

[7] Since June 2004, Cassini has been in orbit around Saturn providing new measurements of the electrons in Saturn's magnetosphere. Two instruments onboard Cassini measure these populations directly, the Electron Spectrometer of the Cassini Plasma Spectrometer (CAPS/ELS) [Young et al., 2004; Linder et al., 1998] and the Low Energy Magnetospheric Measurements System of the Magnetospheric IMaging Instrument (MIMI/LEMMS) [Krimigis et

al., 2004]. Thanks to some overlap of their energy range, the CAPS/ELS and MIMI/LEMMS instruments provide continuous coverage of electron populations from a few eV to a few MeV. In this paper we will focus our analysis on electron populations below 1 keV, i.e., in the energy range of the CAPS/ELS instrument. The CAPS/ELS instrument is an electrostatic analyzer that measures electron count rates from 0.56 eV to 28 keV in 63 logarithmically spaced energy channels. The 8 anodes of the instrument are mounted on a turntable partially rotating around the Z axis of the spacecraft, which allows a spatial coverage of 160° in elevation and 208° in azimuth. The energy resolution ( $\Delta E/E$ ) of the instrument is 16.7%.

[8] To be complete, the particle instruments are not the only instruments able to measure the electrons. The RPWS electric antenna can measure the upper hybrid frequency [Persoon et al., 2005], whereas quasi-thermal noise spectroscopy technique can be used to determine the core and halo electron components in the innermost region of the magnetosphere [Moncuquet et al., 2005]. Finally, the RPWS LP measures with a good accuracy the thermal component in the plasma disc (densities and temperatures [Wahlund et al., 2005, 2009]). Hence, the RPWS data provide additional information on the low-energy electrons (energy lower than 10 eV) not detected by the CAPS/ELS instrument when the Cassini spacecraft potential is negative.

### 2.2. Electron Spectra and Data Correction

[9] In the innermost regions of Saturn's magnetosphere, within 5  $R_s$ , penetrating high-energy particles contaminate the measurements of the CAPS/ELS instrument, with an angle-dependent background count rate due to penetrating radiation observed over all energies in all anodes. This is an effect associated with the presence of Saturn's radiation belts. We correct our data from this background taking advantage of the common energy bandwidth covered by the CAPS/ELS and the MIMI/LEMMS instruments at about 20 keV. Assuming that the MIMI/LEMMS low-energy channels are not affected by high-energy particle contamination [Roussos et al., 2007], the flux of penetrating radiation is defined as the difference of the flux measured by both instruments at 20 keV. The signal noise is set to the root mean square value of the penetrating radiation value. The sum of the penetrating radiation value and the signal noise value is then subtracted from each energy bin of the CAPS/ELS detector.

[10] In addition, spacecraft charging (positive or negative) also affects the measurements of the energy distribution of the particles, by adding an energy offset to the measured phase space density spectrum according to Liouville's theorem. When positive, the spacecraft potential can be determined using CAPS/ELS observations of trapped spacecraft photoelectrons [Lewis et al., 2008] and used in order to correct our measurements. Unfortunately, when negative, such as in the inner regions of Saturn's magnetosphere, the spacecraft potential cannot be determined directly using CAPS/ELS observations alone. In this case, some part of the phase space density distribution is not visible. Cross calibration is however possible using the RPWS measurements [Lewis et al., 2008] and this was done previously to estimate the total density [e.g. Tokar et al., 2006]. In this paper, electron spectra are not adjusted for the spacecraft charging effect because the spacecraft

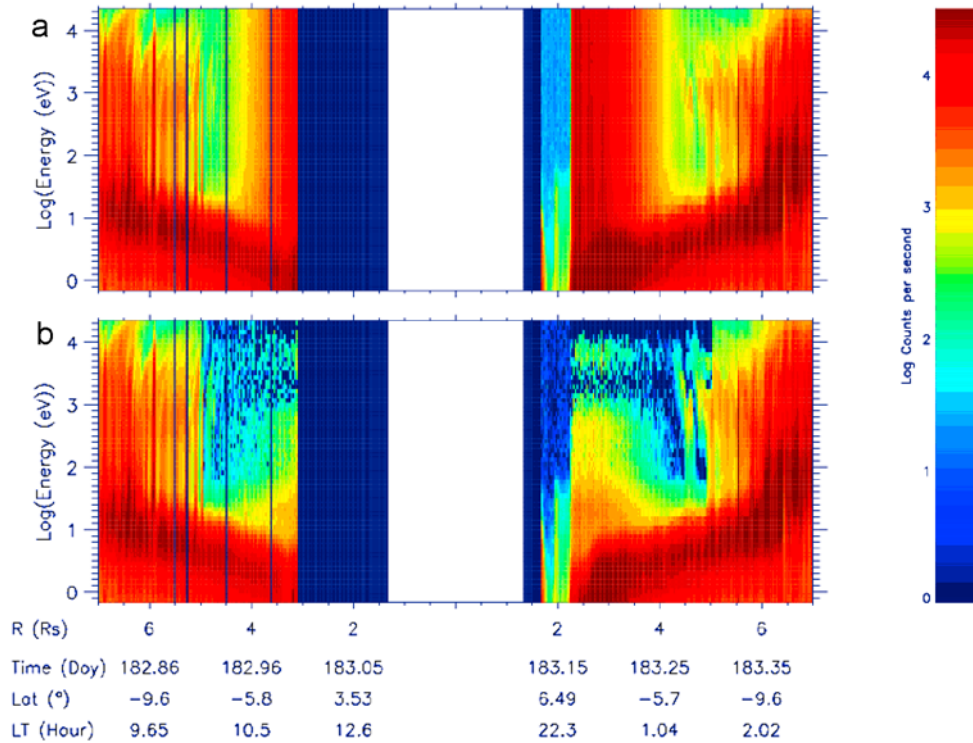


**Figure 1.** Energy (in eV)–radial distance (in  $R_s$ ) spectrogram of electron count rate (in logarithmic scale) from CAPS ELS (Anode 5) during Saturn Orbit Insertion (SOI): (a) before correction for penetrating radiation and (b) after correction for penetrating radiation.

potential is negative and, hence, dependent on other measurements in the regions of interest (e.g., RPWS Langmuir Probe). We will however show how this potential can be estimated where the Saturnian photoelectron peaks are visible in the CAPS/ELS observations reported in the present paper.

### 2.3. Moment Calculation

[11] Our moment calculation is based on the forward modeling method described by Schippers *et al.* [2008]: a bimodal distribution model composed of two isotropic kappa distributions representing the thermal and the suprathermal electron populations respectively, observed everywhere in the magnetosphere [Sittler *et al.*, 1983; Young *et al.*, 2005; Rymer *et al.*, 2007], is adjusted on the CAPS/ELS-MIMI/LEMMS electron composite flux spectra. Although our bimodal model reproduce very well the observations, we should note that it does not account for temperature anisotropies (2–4) of the thermal electrons (0.5–5 eV) reported by RPWS LP observations [Wahlund *et al.*, 2009]. This is nevertheless negligible in comparison to the negative potential issue which affects the thermal population. We used these distributions to derive a set of electron fluid parameters (density  $n$ , temperature  $T$ ) per electron population. This method can be easily extended in the case of additional electron populations. In the present paper, we will show that a bimodal electron description is inadequate in the innermost regions of Saturn’s magnetosphere. We need to include an additional electron population modeled by a Maxwellian distribution function in the 20–50 eV energy range in addition to the thermal and the suprathermal

populations. We derive average densities of this new population.

### 3. Observations

[12] We show in Figure 1 how narrow electron energy peaks can be identified and extracted from the background in CAPS/ELS observations obtained in the innermost regions of the Saturnian magnetosphere. Figure 1 displays electron count rates from CAPS ELS obtained within 10  $R_s$  during the Saturn Orbit Injection (SOI) orbit of the spacecraft around Saturn, in 2004. A qualitative analysis of Figure 1a reveals what appears to be three different electron populations, corresponding to visible energy ranges in the spectrogram. In the innermost magnetosphere ( $\leq 6 R_s$ ), trapped electron radiation belts are observed at very high energy (2 MeV, measured by MIMI, and seen in the ELS data as penetrating radiation across all energies) and their intensity is observed to decrease rapidly as radial distance increases. A bimodal population of electrons at low- (below 100 eV) and intermediate-energy (100 eV–10 keV) is observed by CAPS ELS in most of the magnetosphere [Young *et al.*, 2005]. These electron populations at low- and intermediate-energy correspond to thermal and suprathermal electrons respectively. The coexistence of these two populations in Saturn’s magnetosphere was revealed by Sittler *et al.* [1983] using Voyager PLS observations and then confirmed by Young *et al.* [2005] and Rymer *et al.* [2007] using CAPS observations. Different plasmadisc electron populations have also been observed from RPWS measurements [Moncuquet *et al.*, 2005; Wahlund *et al.*, 2005, 2009; Persoon *et al.*, 2009].

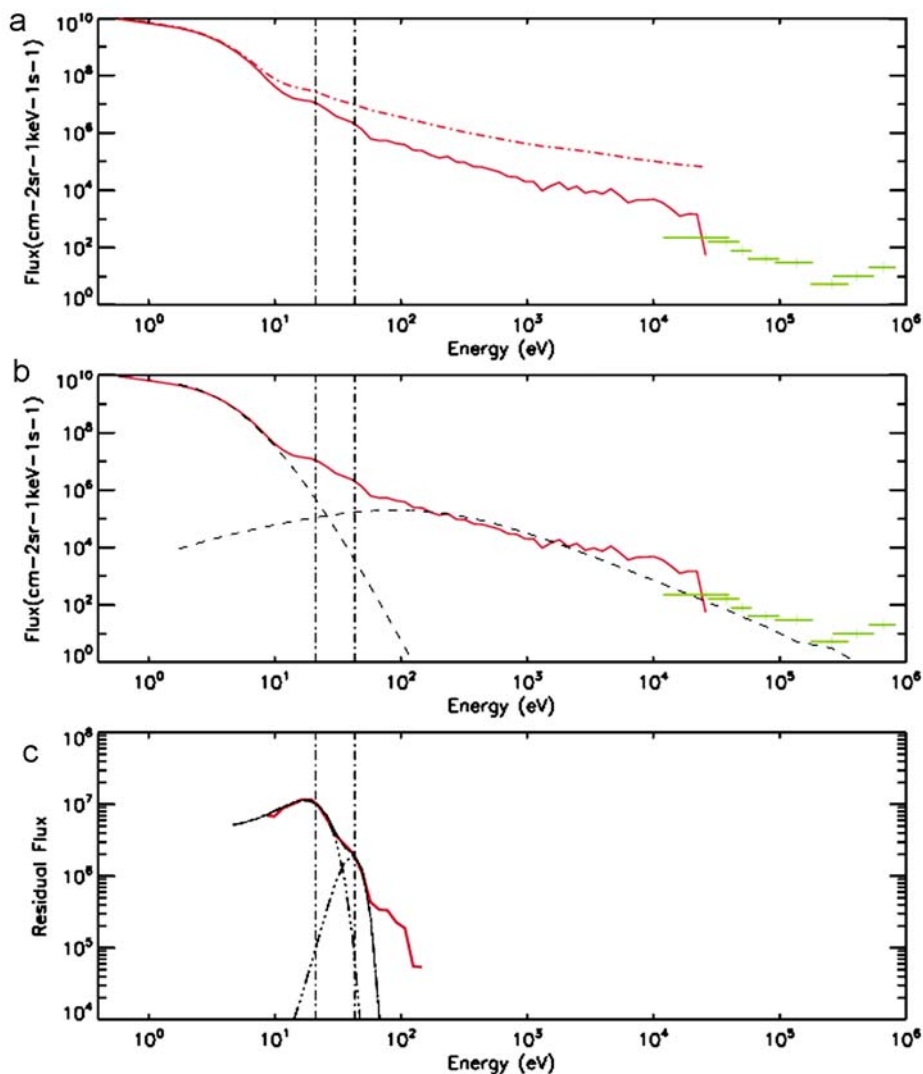


**Figure 2.** (a) Differential number flux spectrum from the combination of CAPS/ELS and MIMI/LEMMS observations obtained by the Cassini spacecraft at  $4.4 R_s$  at 1900 UT on day 104 of year 2005. The CAPS/ELS raw data are displayed as a red dash-dotted line, the CAPS/ELS data are displayed with background subtracted as a red solid line, and the MIMI/LEMMS data are displayed in green. (b) The same as Figure 2a with overlaid thermal and suprathermal kappa models. (c) Residuals of differential number flux after the contributions from the thermal and suprathermal electron populations have been removed. Gaussian distributions are fitted to the two observed narrow peaks (in the 10–100 eV energy range).

[13] We can see in the middle of the plot in Figure 1a the penetrating radiation component of the signal in the detector due to penetrating high-energy particles, that are observed across all CAPS/ELS energies. We then apply the procedure described in section 2.2 in order to remove the penetrating radiation. The end result is illustrated in Figure 1b. This enables us to identify a new and distinct electron population in the 20–50 eV energy band, which was clearly hidden before this correction but it can be readily distinguished in Figures 2a–2c.

[14] We present in Figure 2a composite CAPS/ELS and MIMI/LEMMS (energy channels C0–C7) spectral plots of electron intensities observed at  $4 R_s$  on day 104/2005 (rev 6) versus energy. Figure 2a enables us to illustrate and validate our correction for penetrating radiation. To be complete, we

note the presence of remaining features at near 500 eV and 8 keV even after correction within  $3 R_s$ , where the contamination of the spacecraft is particularly important. These features are however one order less intense than the new features reported before (see Figure 2b). The raw CAPS/ELS fluxes (dash-dotted line in red) are first corrected from high-energy penetrating particles using the method described previously. The corrected CAPS/ELS flux (solid line in red) appears quite consistent with the electron fluxes observed in the MIMI/LEMMS energy range (in green). This observation validates our correction as well as the geometric factors used (G. R. Lewis, In flight calibration of the Cassini-Huygens CAPS electron spectrometer, submitted to *Planetary and Space Science*, 2009). Figure 2a enables us to identify the presence of broad energy peaks corresponding

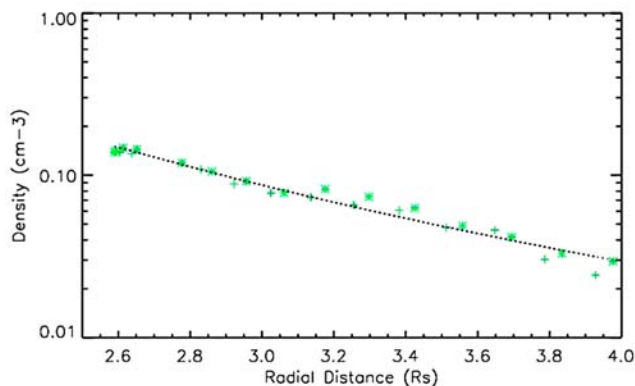


**Figure 3.** Radial profile (in  $R_s$ ) of the electron narrow peak density ( $\text{cm}^{-3}$ ) close to the periapsis of rev 6 (days 104 and 105 of year 2005). (Inbound data are plotted with crosses. Outbound data are plotted with stars). A power law model ( $\propto L^{-n}$ ) adjusted to the density profile with  $n = 3.7$  is superimposed as a dotted line.

to the thermal (a few eV) and suprathermal (above 100 eV) electron populations observed everywhere in Saturn's magnetosphere, together with a narrow and distinct peak at  $\sim 20$  eV and a possible peak at 42 eV (delineated by dash-dotted lines) which taken together will constitute the new electron population whose properties are detailed hereafter. In Figure 2b, the result of our forward modeling for the thermal, suprathermal, and new electron populations (dash-dotted lines) are superimposed on top of the observations. Whereas the new electron population in the 20–50 eV energy range can be clearly observed in this type of representation, its properties appear unambiguously when the residuals of the flux composite spectra (thermal and suprathermal models removed) are displayed, as done in Figure 2c.

[15] The density of our newly identified electron population for the near-equatorial orbit rev 6 (with full CAPS/ELS energy resolution) are shown in Figure 3 (in green), with respect to radial distance. The ratio of density of this new electron population to the total electron density determined from the CAPS/ELS instrument is about 10%. Since the spacecraft potential is negative in the innermost regions of Saturn's magnetosphere, we point out that we underestimate the real density of the electron thermal population (partially detected because of its low temperature, and the moment calculation is uncorrected for the undetermined negative spacecraft potential as discussed earlier). Typical published RPWS results [Persoon *et al.*, 2005] indicate that the total electron density is about ten times our estimation with CAPS and therefore the ratio of the new electron population density to the total electron density from upper hybrid frequency should be close to 1%. In addition, the temperature of this new population evolves little with radial distance (not shown).

[16] Figure 4 provides us with an illustration of the spatial locations where this new electron population is observed. Figure 4a shows the location of this population in the equatorial plane of the KSE coordinate system. Figure 4b shows the location of this population in the meridional plane ( $\rho$ ,  $z_{eq}$ ). For Figure 4, we have chosen orbits with perikrones inside  $4 R_s$  during the time period July 2004 to December 2007. This new population is observed unambig-

uously within  $4-5 R_s$  during all these orbits, at every Local Time and at latitude inside  $2 R_s$  (This last limit is imposed by the orbits chosen). Further studies will be required to constrain the latitudinal extension of this population. The presence of photoelectron peaks in the region beyond  $4-5 R_s$  cannot be tested since these peaks are hidden in the tail of the thermal electron population, within the same energy range.

[17] This new electron population also seems to correspond to the electron population with a mean value of 40 eV between 3 and  $6 R_s$ , detected by Moncuquet *et al.* [2005] using the RPWS dipole antenna during SOI.

[18] In order to identify the source of these photoelectron populations, we now consider their pitch angle distribution. Figure 5 displays the time variation of 21 eV (16th channel of CAPS/ELS) electron pitch angle together with information on the Cassini trajectory during its 28th orbit (day 252 of year 2006, this orbit being chosen because the pitch angle coverage of CAPS/ELS is very good). The pitch angle distribution of 21 eV electrons appears to maximize at  $90^\circ$ ,

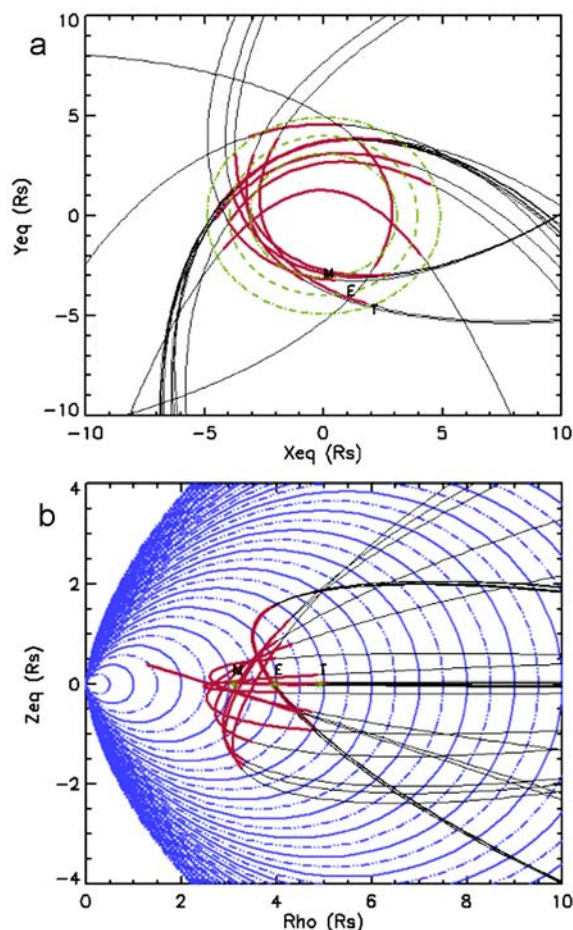


**Figure 4.** Identification of narrow peaks in the Kronocentric Saturn Equatorial coordinate system (KSE). (a) Location of narrow peaks in the equatorial plane (in red on the Cassini trajectory). (b) Location of narrow peaks in the meridional plane (in red). Dipolar magnetic field lines are overlaid in blue. The position of the inner icy satellite orbits (M, Mimas; E, Enceladus; T, Tethys) is overlaid in green (circles in Figure 4a and crosses in Figure 4b).

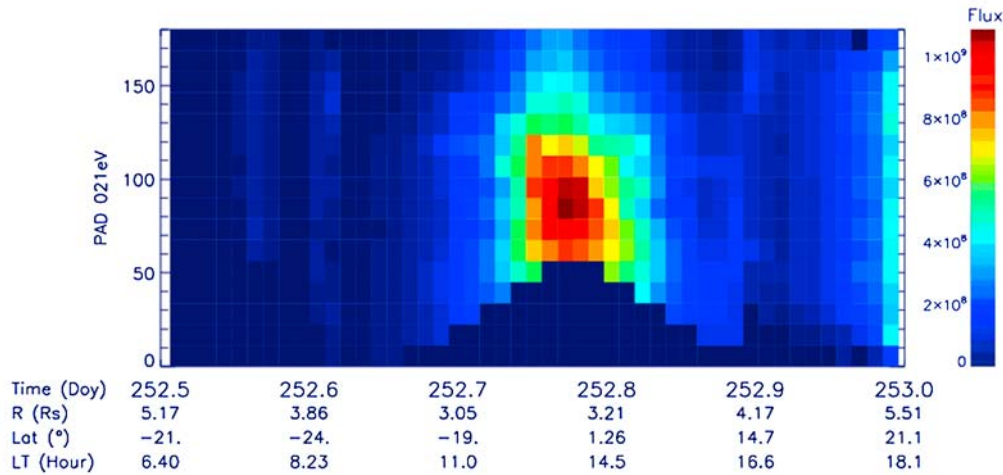


**Figure 5.** Variation of the 21 eV photoelectron pitch angle distribution with time (in day of year) during rev 28 (day 252 of year 2006). Cassini trajectory information (radial distance, latitude, local time) is indicated below the plot.

which indicates an origin close to the equatorial plane rather than in Saturn’s ionosphere which would produce a ‘source cone’ as observed in Earth’s magnetosphere [Coates *et al.*, 1985, and references therein]. These electrons are therefore probably produced in the neutral cloud observed in the inner Saturnian magnetosphere.

#### 4. Model and Discussion

[19] In order to identify the neutral parent species of the observed photoelectrons, we built a synthetic photoelectron spectra using neutral composition and densities of Saturn’s inner neutral cloud given by Jurac and Richardson [2007]. The neutral species that we considered consist of hydroxyl radical  $OH$ , water  $H_2O$ , oxygen  $O$  and hydrogen  $H$ .  $H_2O$  is the dominant neutral species with a density of about  $1000 \text{ cm}^{-3}$  at Enceladus orbit, in the equatorial plane [Jurac and Richardson, 2007]. For each species, we use the table of solar photoionization rate coefficients per wavelength determined by Huebner *et al.* [1992] for planetary atmospheric atomic and molecular components.

[20] We have multiplied the rate coefficients of each neutral species with its density in the neutral cloud according to the Jurac and Richardson model, and summed all contributions to finally compute a photoelectron synthetic spectrum. The resulting model spectrum, directly comparable with the observed one at 1900 UT on day 104 of year 2005, is presented in Figure 6 (the synthetic spectra sampled at CAPS/ELS resolution is overlaid in red) with respect to excess energy ( $hc/\lambda - hc/\lambda_{th}$ , with  $\lambda$ , the wavelength of the solar line and  $\lambda_{th}$ , the threshold ionization wavelength). The peak of maximum energy appears around 28 eV in our synthetic spectrum, together with secondary peaks at lower energies. In addition, above 28 eV, another energy peak is observed in the 48–50 eV energy range. All neutral species contribute to the identified peaks but the intensity of these peaks is largely dominated by the photoionization of  $H_2O$ .

[21] Our photoelectron synthetic spectrum corresponds to photoelectron production. We are fully aware that our observed photoelectrons are the results of an equilibrium

between source, transport and loss processes of ambient electrons, and that a more complete model taking into account all these processes would ideally be needed to understand fully our observations. We simply mention that the main loss process for these newly produced photoelectrons may be the cooling resulting from the interaction with another neutral species.

[22] In order to pursue our simple analysis, we have scaled our synthetic spectrum with our observations, in intensity, and shifted the modeled peak to match the observed one at 20 eV, that we have interpreted to correspond to the modeled 28 eV photoelectron peak.

[23] In Figure 7 we have superimposed the scaled and shifted synthetic spectrum onto the observations displayed in Figure 2. Our interpretation is supported by the following observations. First, the energy delta between the observed

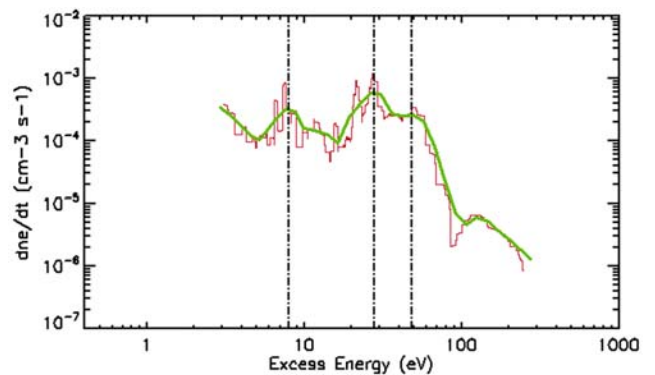


**Figure 6.** Synthetic spectra of photoelectron production ( $\text{cm}^{-3} \text{ s}^{-1}$ ) versus excess energy ( $hc/\lambda - hc/\lambda_{th}$ , with  $\lambda$  being the wavelength of the solar line and  $\lambda_{th}$  being the threshold ionization wavelength). The spectra is built from time constants of the  $O$ ,  $OH$ ,  $H$ ,  $H_2O$  neutral species in the neutral torus [Jurac and Richardson, 2007] (in red). The spectra degraded at the ELS instrument energy resolution (0.17) is superimposed in green. The main peaks are located at 8, 28, and 48 eV (vertical dash-dotted lines).

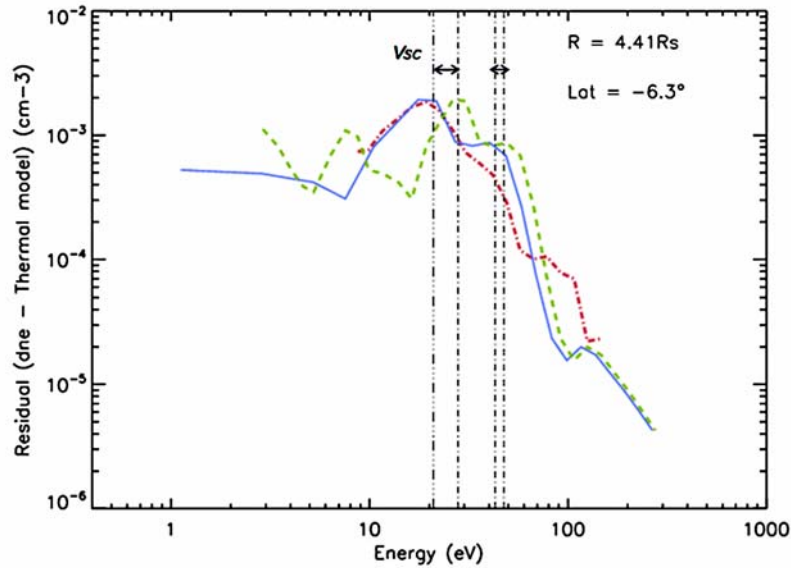


**Figure 7.** Photoelectron partial density spectra  $dne$  ( $\text{cm}^{-3}$ ) at 1900 SCET on day 104 of year 2005. The CAPS/ELS partial density (residual, Figure 2c) is displayed as a red dash-dotted line. The synthetic spectra scaled to the CAPS/ELS observations is displayed as a green dashed line, and the synthetic spectra shifted to the observed narrow peaks is in blue. The spacecraft potential value ( $V_{sc}$ ) could be deduced from the gap between the modeled and the observed energy peaks.

intense narrow peaks at 20 and 45 eV is similar to the energy delta between the modeled synthetic peaks at 28 and 48–50 eV. Second, the relative intensity between the modeled synthetic peaks at 28 and 48–50 eV appears similar to the relative intensity between our observed peaks.

[24] Based on our assumption on the origin of the new electron population, we can use the shift in energy between the observed and the modeled photoelectron energy peak as an estimate of the local spacecraft potential where the CAPS/ELS instrument is located, as done by *Frahm et al.* [2009] and *Coates et al.* [2008] in the Martian and Venusian induced magnetospheres. The photoelectron peak is observed at 20 eV instead of 28 eV, and the second peak is observed at 48 eV peak instead of 42 eV in our synthetic spectrum. The energy difference, between  $-6$  and  $-8$  eV, corresponds to our estimated spacecraft potential, which is negative since we observe the peak at a smaller energy than expected. This value is of the same order of the spacecraft potential measured during Saturn Orbit Insertion by the Langmuir probe onboard Cassini ( $-5$  eV) in the innermost regions of Saturn's magnetosphere [*Wahlund et al.*, 2005; *Jacobsen et al.*, 2009] and derived by intercalibration between the CAPS/ELS density and the density obtained from upper hybrid frequency emissions (G. R. Lewis et al., submitted manuscript, 2009). Such a negative potential is certainly enough to explain the underestimation of the total electron density (mainly supported by electrons of a few eV) derived from the CAPS/ELS observations compared to RPWS observations. The latter are indeed fully independent of spacecraft potential and provide the total plasma density surrounding Cassini. A more thorough comparison between RPWS and CAPS/ELS observations is clearly needed (private communication from one of the referees indicates a value measured by LP of  $-2$  to  $-3$  V at 1900 SCET on day 104 of year 2005) but is beyond the scope of this paper.

[25] It is interesting to note that the radial profile of the near-equatorial density of the new population decreases outwards as  $L^{-n}$  with  $n$  lower than 4 (Figure 3). In the case of pure transport (no source, no sink), the radial profile of the flux tube content  $\eta$  should be constant [*Falthammer*, 1968]. In a fast rotating magnetosphere with dipolar magnetic configuration, the equatorial density would be expected to evolve as  $L^{-4}$  [*Hill and Michel*, 1976]. Therefore, the flux tube content of our new electron population should increase slowly outwards ( $\eta \propto L^{0.3}$ ), at least up to  $4-5 R_s$  (our observational limit). This is consistent with a possible distributed source in the inner magnetosphere peaking at Enceladus, and the  $H_2O$  neutral column density profile derived by *Johnson et al.* [2006a].

## 5. Conclusions

[26] We have identified a new electron population in the low-energy range (20–50 eV) of the CAPS/ELS electron spectra. We have determined the spatial and quantitative properties of this electron population. This population is observed in Saturn's innermost magnetosphere, unambiguously inside  $4-5 R_s$ . Its pitch angle distribution indicates an origin in the equatorial plane, where the extended neutral cloud co-orbits. The newly identified population is characterized by narrow peaks. We used these properties to infer that these narrow peaks are the signature of photoelectrons created by photoionization (solar radiation) of the neutral cloud atoms and molecules. We have tested this assumption by creating synthetic photoelectron spectra from the neutral cloud composition and photoionization time constants. This comparison indicates that the observed and the modeled spectra are similar, within an energy shift of a few eV which we interpret as due partly to the negative spacecraft negative potential. This indicates two useful results: first, if the

components of the neutral cloud are known, then the analysis of photoelectrons could be used to estimate the local spacecraft potential where the CAPS/ELS instrument is located and then compare this with the directly measurable potential in Saturn's magnetosphere innermost regions. Second, in regions where the density of neutrals is unknown, the photoelectron peaks could be used to help determine the neutral densities.

[27] **Acknowledgments.** We thank the Mullard Space Science Laboratory CAPS operations team, L. K. Gilbert and G. R. Lewis, for support in data calibration and correction and STFC for funding in the UK. R.E.J. acknowledges support from Southwest Research Institute for CAPS data analysis. The authors acknowledge NASA/JPL contract 1243218 for financial support of the CAPS investigation.

[28] Amitava Bhattacharjee thanks Michel Moncuquet and Jan-Erik Wahlund for their assistance in evaluating this paper.

## References

- Blanc, M., et al. (2002), Magnetospheric and plasma science with Cassini-Huygens, *Space Sci. Rev.*, *104*(1), 253–346, doi:10.1023/A:1023605110711.
- Coates, A. J., et al. (1985), Ionospheric photoelectrons observed in the magnetosphere at distances of up to 7 Earth radii, *Planet. Space Sci.*, *33*, 1267–1275.
- Coates, A. J., et al. (2005), Plasma electrons above Saturn's main rings: CAPS observations, *Geophys. Res. Lett.*, *32*, L14S09, doi:10.1029/2005GL022694.
- Coates, A. J., et al. (2007), Ionospheric electrons in Titan's tail: Plasma structure during the Cassini T9 encounter, *Geophys. Res. Lett.*, *34*, L24S05, doi:10.1029/2007GL030919.
- Coates, A. J., et al. (2008), Ionospheric photoelectrons at Venus: Initial observations by ASPERA-4 ELS, *Planet. Space Sci.*, *56*(6), 802–806, doi:10.1016/j.pss.2007.12.008.
- Delamere, P. A., and F. Bagenal (2008), Longitudinal plasma density variations at Saturn caused by hot electrons, *Geophys. Res. Lett.*, *35*, L03107, doi:10.1029/2007GL031095.
- Dougherty, M. K., et al. (2006), Identification of a dynamic atmosphere at Enceladus with the Cassini magnetometer, *Science*, *311*, 1406–1409, doi:10.1126/science.1120985.
- Esposito, L., et al. (2005), Ultraviolet imaging spectroscopy shows an active Saturnian system, *Science*, *307*, 1251–1255, doi:10.1126/science.1105606.
- Falthammar, C. G. (1968), Radial diffusion by violation of the third adiabatic invariant, in *Earth's Particles and Fields*, edited by B. M. McCormac, pp. 157–169, Reinhold, N. Y.
- Farrell, L., et al. (2008), Mass unloading along the inner edge of the Enceladus plasma torus, *Geophys. Res. Lett.*, *35*, L02203, doi:10.1029/2007GL032306.
- Frahm, R. A., et al. (2006), Carbon dioxide photoelectron energy peaks at Mars, *Icarus*, *182*(2), 371–382, doi:10.1016/j.icarus.2006.01.014.
- Frahm, R. A., et al. (2009), Estimation of the escape of photoelectrons from Mars in 2004 liberated by the ionization of carbon dioxide and atomic oxygen, *Icarus*, doi:10.1016/j.icarus.2009.03.024, in press.
- Hansen, C., et al. (2006), Enceladus' water vapor plume, *Science*, *311*, 1422–1425, doi:10.1126/science.1121254.
- Hill, T. W., and F. C. Michel (1976), Heavy ions from the Galilean satellites and the centrifugal distortion of the Jovian magnetosphere, *J. Geophys. Res.*, *81*, 4561–4565.
- Huebner, W. F., J. J. Keady, and S. P. Lyon (1992), *Solar Photo Rates for Planetary Atmospheres and Atmospheric Pollutants*, *Astrophys. Space Sci.*, vol. 195, pp. 1–289, 291–294, Kluwer Acad., Dordrecht, Netherlands.
- Jacobsen, K. S., J.-E. Wahlund, and A. Pedersen (2009), Cassini Langmuir probe measurements in the inner magnetosphere of Saturn, *Planet. Space Sci.*, *57*, 48–52, doi:10.1016/j.pss.2008.10.012.
- Johnson, R. E., et al. (2006a), The Enceladus and OH tori at Saturn, *Astrophys. J.*, *644*, L137–L139, doi:10.1086/505750.
- Johnson, R. E., et al. (2006b), Production, ionization and redistribution of O<sub>2</sub> in Saturn's ring atmosphere, *Icarus*, *180*, 393–402, doi:10.1016/j.icarus.2005.08.021.
- Jurac, S., and J. D. Richardson (2007), Neutral cloud interaction with Saturn's main rings, *Geophys. Res. Lett.*, *34*, L08102, doi:10.1029/2007GL029567.
- Jurac, S., et al. (2001), Saturn's E ring and production of the neutral torus, *Icarus*, *149*, 384–396, doi:10.1006/icar.2000.6528.
- Krimigis, S. M., et al. (2004), Magnetosphere Imaging Instrument (MIMI) on the Cassini Mission to Saturn/Titan, *Space Sci. Rev.*, *114*, 233–329, doi:10.1007/s11214-004-1410-8.
- Lewis, G. R., et al. (2008), Derivation of density and temperature from the Cassini-Huygens CAPS electron spectrometer, *Planet. Space Sci.*, *56*, 901–912, doi:10.1016/j.pss.2007.12.017.
- Linder, D. R., et al. (1998), The Cassini CAPS electron spectrometer, in *Measurement Techniques in Space Plasmas: Particles*, *Geophys. Monogr. Ser.*, vol. 102, edited by R. E. Pfaff, J. E. Borovsky, and D. T. Young, pp. 257–262, AGU, Washington, D. C.
- Moncuquet, M., et al. (2005), Quasi thermal noise spectroscopy in the inner magnetosphere of Saturn with Cassini/RPWS: Electron temperatures and density, *Geophys. Res. Lett.*, *32*, L20S02, doi:10.1029/2005GL022508.
- Persoon, A. M., et al. (2005), Equatorial electron density measurements in Saturn's inner magnetosphere, *Geophys. Res. Lett.*, *32*, L23105, doi:10.1029/2005GL024294.
- Persoon, A. M., et al. (2009), A diffusive equilibrium model for the plasma density in Saturn's magnetosphere, *J. Geophys. Res.*, *114*, A04211, doi:10.1029/2008JA013912.
- Porco, C., et al. (2006), Cassini observes the active south pole of Enceladus, *Science*, *311*, 1393–1401, doi:10.1126/science.1123013.
- Roussos, E., G. H. Jones, N. Krupp, C. Paranicas, D. G. Mitchell, A. Lagg, J. Woch, U. Motschmann, S. M. Krimigis, and M. K. Dougherty (2007), Electron microdiffusion in the Saturnian radiation belts: Cassini MIMI/LEMMS observations of energetic electron absorption by the icy moons, *J. Geophys. Res.*, *112*, A06214, doi:10.1029/2006JA012027.
- Rymer, A. M., et al. (2007), Electron sources in Saturn's magnetosphere, *J. Geophys. Res.*, *112*, A02201, doi:10.1029/2006JA012017.
- Santos-Costa, D., et al. (2007), Examining the dynamics of low-energy electrons in Saturn's magnetosphere by combining Cassini CAPS-ELS data with charged particle transport model, *Eos Trans. AGU*, *88*, 52, Fall Meet. Suppl., Abstract P43A-1027.
- Schippers, P., et al. (2008), Multi-instrument analysis of electron populations in Saturn's magnetosphere, *J. Geophys. Res.*, *113*, A07208, doi:10.1029/2008JA013098.
- Shemansky, D. E., and D. T. Hall (1992), The distribution of atomic hydrogen in the magnetosphere of Saturn, *Geophys. Res. Lett.*, *97*, 4143–4161.
- Shemansky, D. E., et al. (1993), Detection of the hydroxyl radical in the Saturn magnetosphere, *Nature*, *363*, 329–331.
- Sittler, E. C., Jr., K. W. Olgvie, and J. D. Scudder (1983), Survey of low-energy plasma electrons in Saturn's magnetosphere: Voyager 1 and 2, *J. Geophys. Res.*, *88*, 8847–8870.
- Tokar, R. L., et al. (2005), Cassini observations of the thermal plasma in the vicinity of Saturn's main rings and the F and G rings, *Geophys. Res. Lett.*, *32*, L14S04, doi:10.1029/2005GL022690.
- Tokar, R. L., et al. (2006), The interaction of the atmosphere of Enceladus with Saturn's plasma, *Science*, *311*, 1409–1412, doi:10.1126/science.1121061.
- Tokar, R. L., et al. (2008), Cassini detection of water-group pick-up ions in the Enceladus torus, *Geophys. Res. Lett.*, *35*, L14202, doi:10.1029/2008GL034749.
- Wahlund, J. E., et al. (2005), The inner magnetosphere of Saturn: Cassini RPWS cold plasma results from the first encounter, *Geophys. Res. Lett.*, *32*, L20S09, doi:10.1029/2005GL022699.
- Wahlund, J. E., et al. (2009), Detection of dusty plasma near the E-ring of Saturn, *Planet. Space Sci.*, doi:10.1016/j.pss.2009.03.011, in press.
- Young, D. T., et al. (2004), *Cassini Plasma Spectrometer Investigation*, *Space Sci. Rev.*, vol. 114, 112 pp., doi:10.1007/s11214-004-1406-4, Springer, Dordrecht, Netherlands.
- Young, D. T., et al. (2005), Composition and dynamics of plasma in Saturn's magnetosphere, *Science*, *307*, 1262–1266, doi:10.1126/science.1106151.

N. André, Research and Scientific Support Department, SRE-SM, ESTEC, European Space Agency, Keplerlaan 1, NL-2200 AG Noordwijk, Netherlands.

M. Blanc and I. Dandouras, Centre d'Etude Spatiale des Rayonnements, 9 av. du Colonel Roche, F-31028 Toulouse, France.

A. J. Coates, Mullard Space Science Laboratory, University College London, Surrey RH5 6NT, UK.

R. E. Johnson, Engineering Physics, University of Virginia, Charlottesville, VA 22904, USA.

S. M. Krimigis, Johns Hopkins University Applied Physics Laboratory, 11100 Johns Hopkins Rd., Laurel, MD 20723-6099, USA.

P. Schippers, Department of Physics and Astronomy, University of Iowa, 203 Van Allen Hall, Iowa City, IA 52242-1479, USA. (patricia-schippers@uiowa.edu)

D. T. Young, Southwest Research Institute, San Antonio, TX 78238, USA.